Article

Neuron

Molecular Tuning of the Axonal Mitochondrial Ca^{2+} Uniporter Ensures Metabolic Flexibility of Neurotransmission

Graphical Abstract

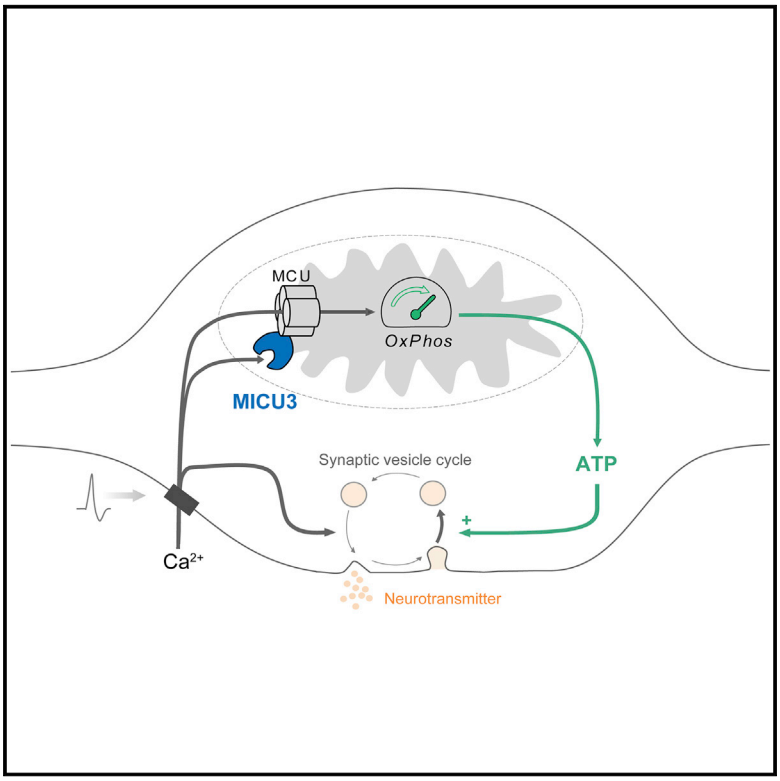

Authors

Ghazaleh Ashrafi, Jaime de Juan-Sanz, Ryan J. Farrell, Timothy A. Ryan

Correspondence

taryan@med.cornell.edu

In Brief

Nerve terminals in the brain must synthesize ATP on demand to sustain function. Here, Ashrafi, de Juan-Sanz, et al. show that axonal mitochondria use the brain-specific MCU regulator MICU3 to allow efficient Ca^{2+} uptake in order to accelerate ATP production.

Highlights

- Synapses rely on activity-driven mitochondrial ATP synthesis under oxidative conditions
- Mitochondrial Ca^{2+} uptake is required to stimulate ATP synthesis in axons
- The mitochondria Ca^{2+} uptake threshold is lower in axons than in non-neuronal cells
- MICU3 controls the Ca^{2+} sensitivity of MCU in axonal mitochondria

Ashrafi et al., 2020, Neuron *105*, 1–10
February 19, 2020
https://doi.org/10.1016/j.neuron.2019.11.020

CellPress

Please cite this article in press as: Ashrafi et al., Molecular Tuning of the Axonal Mitochondrial Ca^{2+} Uniporter Ensures Metabolic Flexibility of Neurotransmission, Neuron (2019), https://doi.org/10.1016/j.neuron.2019.11.020

Neuron
Article

Molecular Tuning of the Axonal Mitochondrial Ca^{2+} Uniporter Ensures Metabolic Flexibility of Neurotransmission

Ghazaleh Ashrafi,[1,3,5] Jaime de Juan-Sanz,[1,3,4] Ryan J. Farrell,[1,2] and Timothy A. Ryan[1,6,*]
[1]Department of Biochemistry, Weill Cornell Medicine, New York, NY 10065, USA
[2]David Rockefeller Graduate Program, Rockefeller University, New York, NY 10065, USA
[3]These authors contributed equally
[4]Present address: Sorbonne Université and Institut du Cerveau et de la Moelle Epinière (ICM), Hôpital Pitié-Salpêtrière, Inserm, CNRS, Paris, France
[5]Present address: Department of Cell Biology and Physiology and Department of Genetics, Washington University School of Medicine in St. Louis, St. Louis, MO 63110, USA
[6]Lead Contact
*Correspondence: taryan@med.cornell.edu
https://doi.org/10.1016/j.neuron.2019.11.020

SUMMARY

The brain is a vulnerable metabolic organ and must adapt to different fuel conditions to sustain function. Nerve terminals are a locus of this vulnerability, but how they regulate ATP synthesis as fuel conditions vary is unknown. We show that synapses can switch from glycolytic to oxidative metabolism, but to do so, they rely on activity-driven presynaptic mitochondrial Ca^{2+} uptake to accelerate ATP production. We demonstrate that, whereas mitochondrial Ca^{2+} uptake requires elevated extramitochondrial Ca^{2+} in non-neuronal cells, axonal mitochondria readily take up Ca^{2+} in response to small changes in external Ca^{2+}. We identified the brain-specific protein MICU3 as a critical driver of this tuning of Ca^{2+} sensitivity. Ablation of MICU3 renders axonal mitochondria similar to non-neuronal mitochondria, prevents acceleration of local ATP synthesis, and impairs presynaptic function under oxidative conditions. Thus, presynaptic mitochondria rely on MICU3 to facilitate mitochondrial Ca^{2+} uptake during activity and achieve metabolic flexibility.

INTRODUCTION

In humans, when blood glucose drops below ~2.8 mM, severe neurological consequences ensue, including delirium and coma (Posner et al., 2007). The brain is uniquely sensitive to fuel availability, as neurons do not store significant reserves of high-energy molecules and the brain does not appear to carry out β-oxidation (Schönfeld and Reiser, 2013). In addition, the concentration of glucose in human cerebrospinal fluid (CSF) is typically two-thirds of that in blood (Seehusen et al., 2003), whereas in rodent, glucose CSF is considerably lower (~1 mM) than that of blood (~5 mM when fasting) (McNay and Gold, 1999). There is accumulating evidence that the brain is capable of adapting to different fuel sources (Vannucci and Vannucci, 2000). For example, a restrictive ketogenic diet is the main therapeutic approach for the treatment of drug-resistant childhood epilepsies (Neal et al., 2008), and chronic blockade of mitochondrial pyruvate uptake makes neurons more reliant on glutamate as a driver of the tricarboxylic acid (TCA) cycle (Divakaruni et al., 2017). However, regardless of the fuel source, because neurons cannot store high-energy molecules, they must synthetize ATP on demand to fuel their energetically demanding neurophysiological processes. This coupling of activity and ATP production is particularly constrained at nerve terminals, as they typically operate hundreds of microns or even tens of centimeters away from the cell soma. In support of this view, we previously showed that presynaptic terminals must locally synthesize ATP during activity to meet increased energetic demands (Ashrafi et al., 2017; Rangaraju et al., 2014). Although the brain generally relies exclusively on the delivery of glucose from the body's other organs to sustain function, the extent to which neurons and synapses rely on glycolytic versus oxidative production of ATP has long been debated (Yellen, 2018). The glycolytic machinery is present in nerve terminals, as 5 of the 10 enzymes required for glycolysis are enriched on synaptic vesicles (SVs) (Ikemoto et al., 2003; Knull and Fillmore, 1985), including those that produce ATP. We recently showed that glycolysis in nerve terminals can be upregulated in response to activity by AMP-kinase (AMPK)-driven insertion of GLUT4 glucose transporters into the presynaptic plasma membrane, providing an important link connecting supply and demand for ATP at nerve terminals. Whether the glycolytic production of ATP is enough to sustain function will depend on the local glycolytic capacity, which can be limited by the abundance of glycolytic enzymes, the availability of glucose as substrate, or both. If the glycolytic capacity is limited, then pyruvate produced either by local glycolysis or from lactate supplied by extra-neuronal sources, such as astrocytes (Pellerin et al., 1998), could, in principle, fuel local mitochondria to meet ATP demands. However, how synapses might upregulate ATP production under such oxidative conditions remains unknown (i.e., how can synapses maintain metabolic flexibility while preserving activity-dependent ATP production?). To

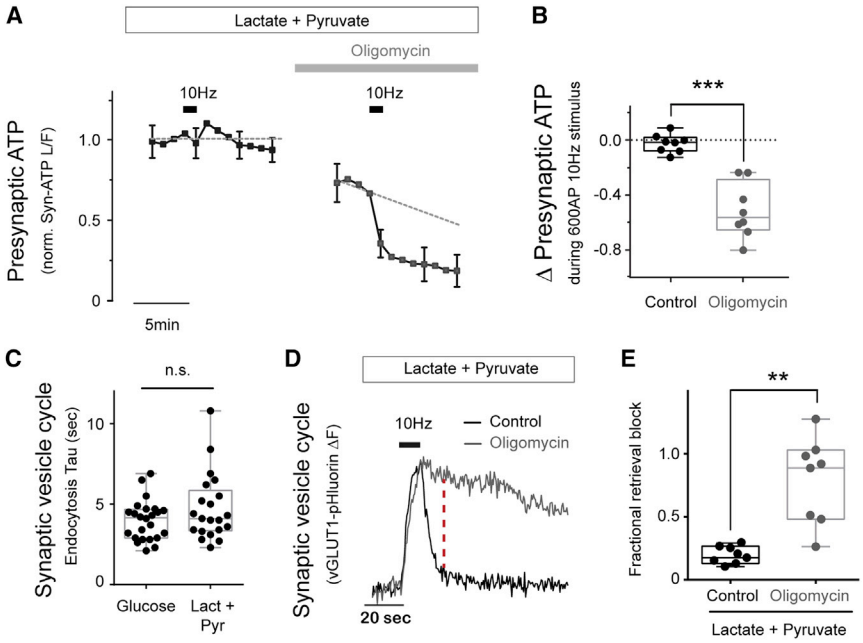

Figure 1. Activity-Driven Mitochondrial ATP Production in Nerve Terminals

(A) Average normalized traces of presynaptic ATP measured with the luminescent reporter Syn-ATP. Neurons were electrically stimulated with 600 action potentials (APs) at 10 Hz (black bar) before and after a 5-min treatment with oligomycin A in the presence of lactate and pyruvate but with no glucose. The gray dashed line represents the normalized ATP value of 1, except for the case in which oligomycin A is added, where it represents the linear fitting to the points prior to stimulation.

(B) Change in normalized ATP levels immediately after stimulation (n = 8 cells). Average change in ATP ± SEM: control, −0.02 ± 0.02; oligomycin, −0.51 ± 0.07.

(C) Endocytosis time constants (tau) of vGLUT1-pH in neurons stimulated in the presence of glucose or lactate and pyruvate. n = 21–24 cells. Average tau (s) ± SEM; glucose, 4.0 ± 0.3; lact+pyr, 4.8 ± 0.5.

(D) Sample vGLUT1-pH traces in response to 100 APs at 10 Hz (black bar) before and 5 min after oligomycin A treatment in the presence of lactate and pyruvate.

(E) Fractional retrieval was calculated as the fraction of vGLUT1-pH signal remaining after 2 times the endocytic constant of control (red dashed line in D) after stimulation (0 and 1 denote complete and no endocytosis, respectively). See STAR Methods. n = 8 cells. Average fractional retrieval ± SEM: control, 0.2 ± 0.02; oligomycin A, 0.8 ± 0.2. Error bars indicate SEM. **p < 0.01, ***p < 0.001, Mann-Whitney U test. n.s., not statistically significant. The box-whisker plot represents median (line), 25th–75th percentile (box), and min–max (whisker).

answer this fundamental question, we examined the regulation of local ATP production during electrical activity in nerve terminals when the carbon source for ATP generation was switched from extracellular glucose to extracellular lactate and pyruvate. We show that rather than a feedback mechanism, such as the one used to upregulate glycolysis, under oxidative conditions, nerve terminals rely on a feedforward mechanism via mitochondrial Ca^{2+} uptake to accelerate ATP production. Classic experiments using a first-generation genetically encoded and mitochondrially targeted Ca^{2+} indicator (Rizzuto et al., 1993) demonstrated that Ca^{2+} uptake into mitochondria likely occurs only at sites of close apposition between an intracellular Ca^{2+} store (e.g., the endoplasmic reticulum [ER]) and mitochondria, consistent with *in vitro* data demonstrating that mitochondria do not readily take up Ca^{2+} unless exposed to high Ca^{2+} concentrations (Sparagna et al., 1994). We show that presynaptic mitochondria, in contrast to those in non-neuronal cells, have a much lower threshold for Ca^{2+} uptake. This property is conveyed by MICU3, a brain-specific regulator of the mitochondrial Ca^{2+} uniporter (MCU), which frees axonal mitochondria from the constraint of relying on an intracellular Ca^{2+} store for Ca^{2+} uptake. In the absence of either MICU3 or MCU, the metabolic plasticity of presynaptic terminals is diminished, resulting in impairment of synaptic function.

RESULTS

Upregulation of Mitochondrial ATP Synthesis during Electrical Activity at Nerve Terminals

We previously demonstrated that nerve-terminal ATP consumption and production is balanced during activity to sustain function (Ashrafi et al., 2017; Rangaraju et al., 2014). Subsequent experiments showed that ATP synthesis can be upregulated by increasing glucose uptake in nerve terminals (Ashrafi et al., 2017), increasing local glycolysis. Increasing glycolysis implies that production of pyruvate, the primary fuel for oxidative phosphorylation, would also accelerate. In order to determine whether mitochondria upregulate ATP synthesis independent of changes in substrate, we monitored ATP levels in nerve terminals of dissociated primary hippocampal neurons using Syn-ATP, a genetically encoded and presynaptically targeted ATP indicator (Rangaraju et al., 2014), and replaced glucose with a mixture of lactate and pyruvate. Robust action potential (AP) firing (600 AP at 10 Hz) under these conditions did not impact ATP levels (Figures 1A and 1B), similar to what we found under glycolytic conditions. Because this level of activity leads to significant ATP consumption (Rangaraju et al., 2014), this result implies that even under purely oxidative conditions, ATP consumption is completely compensated by increasing ATP production. To test this hypothesis, we repeated our experiments blocking mitochondrial ATP production using the F_1-F_0 ATP synthase inhibitor oligomycin A. Under these conditions, we observed an abrupt drop in ATP levels during AP firing (Figures 1A and 1B).

These experiments show that axonal mitochondria respond to electrical activity by upregulating ATP production to precisely match the increased demand for energy. In order to determine whether this acceleration in mitochondrial ATP synthesis is important to sustain nerve-terminal function, we monitored AP-driven SVs' exocytosis, endocytosis, and reacidification using vGLUT1-pHluorin (vGLUT1-pH) (Voglmaier et al., 2006). Replacing extracellular glucose with a mixture of lactate and

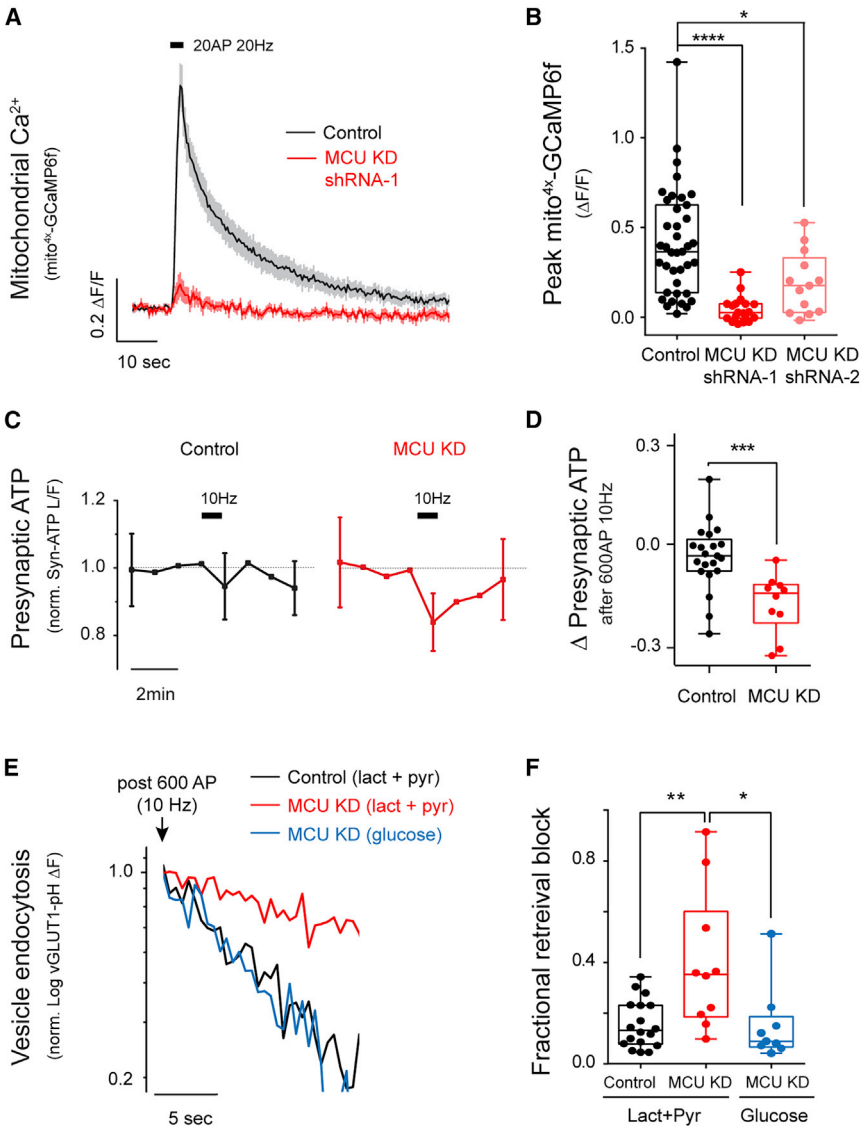

Figure 2. MCU Is Required for Mitochondrial Ca^{2+} Uptake and Activity-Driven ATP Production

(A) Average traces of mito^{4x}-GCaMP6f showing mitochondrial Ca^{2+} uptake in control and MCU KD axons stimulated with 20 AP at 20 Hz. Error bars indicate SEM. n = 19–39 cells.

(B) Peak responses of Mito^{4x}-GCaMP6f (ΔF/F) following stimulation. n = 13–39 cells. Mean ΔF/F ± SEM: control, 0.41 ± 0.05; MCU KD (shRNA-1), 0.04 ± 0.02; MCU KD (shRNA-2), 0.19 ± 0.05. Henceforth, MCU KD refers to MCU KD with shRNA-1. Error bars indicate SEM. ****p < 0.0001, Kruskal-Wallis H Test.

(C and D) Normalized presynaptic ATP traces (C) in control and MCU KD neurons stimulated with 600 AP at 10 Hz. The gray dashed line represents the normalized ATP value of 1. (D) Change in normalized ATP levels immediately after stimulation. n = 9–21 cells. Average change in ATP ± SEM: control, −0.04 ± 0.02; MCU KD, −0.17 ± 0.03. Error bars indicate SEM. ***p < 0.001, Mann-Whitney U test.

(E and F) Sample semi-log plot of vGLUT1-pH traces (E) following stimulation with 600 AP at 10 Hz in control (black) and MCU KD neurons (red) supplied with lactate and pyruvate. Blue trace shows the response of the same MCU KD neuron shown in red but in the presence of media containing glucose. (F) Fractional retrieval block calculated as described in STAR Methods. n = 9–18 cells. Average fractional retrieval ± SEM: control, 0.16 ± 0.02; MCU KD (lact+pyr), 0.40 ± 0.09; MCU KD (glucose), 0.15 ± 0.05. Unless otherwise indicated, all experiments were performed in the presence of lactate and pyruvate. *p < 0.05, **p < 0.01, ***p < 0.001, ****p < 0.0001, Kruskal-Wallis H Test, and Wilcoxon matched-pairs test for comparison between MCU KD (lact+pyr) and MCU KD (glucose). The box-whisker plot represents median (line), 25th–75th percentile (box), and min–max (whisker).

pyruvate has no impact on the kinetics of SV recycling (Figure 1C), demonstrating that synapses have a profound metabolic flexibility with respect to the fuel source. Acute blockade of mitochondrial ATP production under these conditions, however, leads to a complete arrest of SV recycling (Figures 1D and 1E), as expected, because nerve terminals completely rely on oxidative fuel production under these conditions. Thus, as with glycolytic conditions, nerve terminals also upregulate ATP synthesis under oxidative conditions but in this case by accelerating mitochondrial function.

MCU Is Required for Presynaptic Mitochondrial Uptake and Acceleration of ATP Production under Oxidative Conditions

It has long been hypothesized that mitochondrial ATP production is accelerated by Ca^{2+} uptake into mitochondria (Heineman and Balaban, 1990), although detailed tests of this hypothesis in intact cells have been lacking. We took advantage of the identification of the principal molecular component responsible for mitochondrial Ca^{2+} uptake, the MCU (Baughman et al., 2011; De Stefani et al., 2011), to see whether presynaptic mitochondrial Ca^{2+} uptake during activity is necessary to accelerate ATP production. We monitored mitochondrial Ca^{2+} uptake in axons during AP firing (Figure 2A) using an improved mitochondrial-targeting of GCaMP6f (mito^{4x}-GCaMP6f; see STAR Methods). As all GCaMPs are also sensitive to pH, we verified that the stimulus levels used did not impact mitochondrial pH using mito^{4x}-pHluorin (Figure S1A). Even brief bursts of AP firing leads to very robust Ca^{2+} uptake in axonal mitochondria (Figures 2A and 2B). This uptake was suppressed when expression of MCU was transiently knocked down using either of two short hairpin RNA (shRNA) constructs targeting different regions of MCU (Figures 2A and 2B). The most potent construct, MCU KD shRNA-1, hereby referred to as MCU KD, was used for further experiments. The knockdown of *mcu* mRNA was also validated by qPCR (Figure S1B). This block in mitochondrial

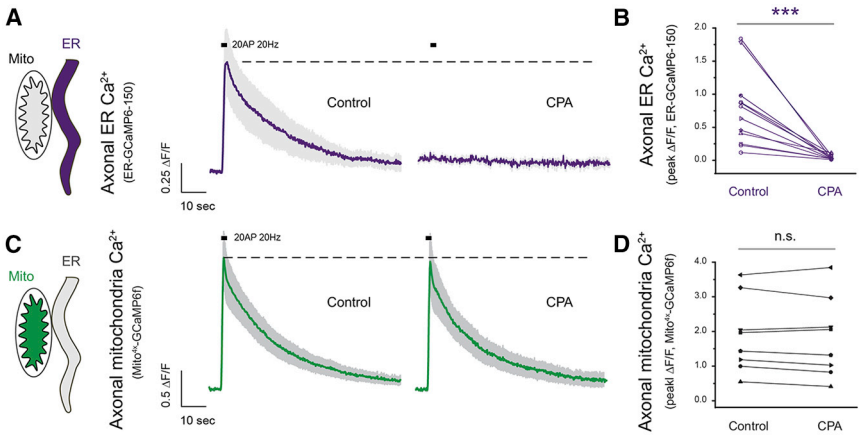

Figure 3. Axonal Mitochondria Do Not Rely on the ER for Ca^{2+} Uptake

(A) Average traces of ER-GCaMP6-150 showing ER Ca^{2+} responses in control neurons and neurons treated with the SERCA inhibitor CPA to silence ER Ca^{2+} uptake.

(B) Paired comparison of peak ER-GCaMP6-150 ΔF/F responses before and after CPA treatment. n = 12 cells. Mean peak ER Ca^{2+} response (ΔF/F) ± SEM: control, 0.77 ± 0.16; CPA-treated, 0.04 ± 0.01.

(C) Average traces of mito^{4x}-GCaMP6f in control and CPA-treated neurons.

(D) n = 8 cells. Average peak mitochondrial Ca^{2+} response (ΔF/F): control, 1.88 ± 0.38; CPA-treated, 1.82 ± 0.41. Experiments were performed in the presence of glucose. Error bars in traces indicate SEM. ***$p < 0.001$, n.s., not statistically significant, Wilcoxon signed ranked test.

Ca^{2+} uptake is consistent with previous work conclusively demonstrating that MCU is the primary rapid uptake pathway for Ca^{2+} in mitochondria (Pan et al., 2013). MCU knockdown, however, did not significantly impact resting mitochondrial matrix Ca^{2+} levels (Figure S1C). We found that neurons do not tolerate overexpression of MCU, consistent with previous reports that overexpression of MCU increases excitotoxicity in neurons (Qiu et al., 2013). Similarly, when attempting to rescue MCU knockdown with a shRNA-insensitive variant of MCU, only few neurons survived. Those that did had partially restored mitochondrial Ca^{2+} uptake (Figure S1D).

Many lines of evidence support the idea that mitochondrial Ca^{2+} uptake can accelerate the TCA cycle to enhance ATP production (Glancy and Balaban, 2012). Because ablation of MCU severely impairs mitochondrial Ca^{2+} uptake, we measured ATP levels at synapses during 1 min of AP firing in neurons that lack MCU. Unlike control neurons, where ATP levels are unperturbed by activity, in the absence of MCU, ATP levels declined during the period of activity and slowly recovered (Figures 2C and 2D). Loss of MCU, however, is not equivalent to blocking the F_1-F_0 ATP synthase (Figures 1A and 1B). These experiments demonstrate that axonal mitochondrial Ca^{2+} uptake is specifically needed to stimulate ATP synthesis during robust neuronal activity. In order to determine whether the inability to accelerate ATP synthesis during activity impacts nerve terminal function, we measured the kinetics of SV recycling using vGLUT1-pH as above. These experiments show that in neurons where MCU is knocked down with either of two different shRNA constructs, SV endocytosis and reacidification are slowed (Figures 2E, 2F, and S1E), whereas exocytosis is not significantly perturbed (Figure S1F). These experiments are carried out under purely oxidative conditions (lactate and pyruvate, zero glucose) where all new ATP synthesis depends on oxidative phosphorylation. In principle, synaptic dysfunction in the absence of MCU might have arisen from downstream consequences of chronic mitochondrial dysfunction. However, simply replacing the fuel source with glucose completely restored synaptic function even with MCU knockdown (Figures 2E and 2F). Thus, loss of MCU-mediated Ca^{2+} uptake impairs synapse function under oxidative, but not glycolytic, conditions, implying that the defects are not pleiotropic in nature. These experiments indicate that MCU is required for the ability of nerve terminals to effectively upregulate mitochondrial ATP production in switching from glycolytic to oxidative conditions.

Presynaptic Mitochondria Do Not Rely on the ER as a Source of Ca^{2+} Uptake

Mitochondrial Ca^{2+} uptake is activated by Ca^{2+} but is thought to be highly constrained, requiring Ca^{2+} levels that would only be satisfied when mitochondria are in close apposition to a Ca^{2+} release site, such as IP_3 receptors or Ryanodine receptors, on the endoplasmic or sarcoplasmic reticulum. This idea is supported by the fact that isolated mitochondria only take up Ca^{2+} when perfused with high Ca^{2+} concentrations (Gunter et al., 1994) and the observation that perfusion of permeabilized cells with IP_3 triggers mitochondrial Ca^{2+} uptake, whereas perfusion of sub-micromolar Ca^{2+} does not (Rizzuto et al., 1993). This cooperation between mitochondria and the ER would therefore implicate the latter organelle in playing a critical role in controlling Ca^{2+}-mediated regulation of oxidative phosphorylation.

In order to determine whether the ER plays such a role in activity-driven mitochondrial Ca^{2+} uptake in axons, we examined mitochondrial Ca^{2+} uptake before and after blocking ER Ca^{2+} handling (Figure 3). During AP firing, the axonal ER in these neurons acts as a net sink for Ca^{2+} (Figure 3A), as we previously demonstrated using a new genetically encoded and ER-targeted Ca^{2+} sensor based on GCaMP6 but with an affinity altered to more closely match the resting ER Ca^{2+} level (de Juan-Sanz et al., 2017). Inhibition of the sarco/endoplasmic reticulum Ca^{2+} ATPase (SERCA) with cyclopiazonic acid (CPA) eliminates ER Ca^{2+} signaling (Figures 3A and 3B) because, in the absence of SERCA activity, Ca^{2+} leaks out of the ER. We previously showed that following the SERCA block, ER Ca^{2+} decreases with a time constant of < 1 min under these conditions (de Juan-Sanz et al., 2017). Mitochondrial Ca^{2+} uptake, however, was unaffected by the SERCA blockade when probed several minutes after CPA addition (Figures 3C and 3D), indicating that activity-driven mitochondrial Ca^{2+} uptake does not depend on the ER to satisfy potential constraints in Ca^{2+}-dependent MCU activation.

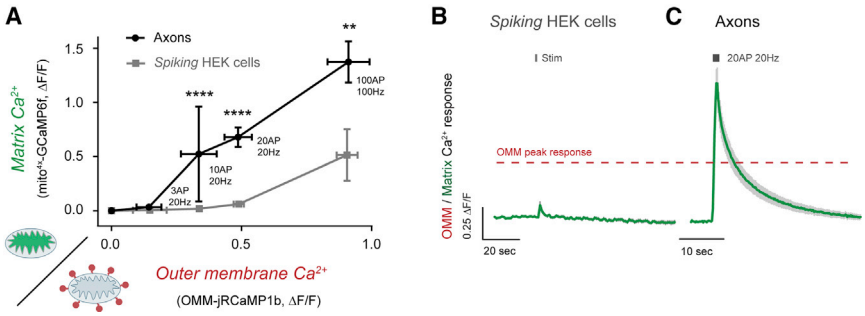

Figure 4. Lower Ca^{2+} Levels Are Needed to Trigger Mitochondrial Ca^{2+} Uptake in Nerve Terminals Than in Non-neuronal Cells

(A–C) Correlation of the mitochondrial matrix-targeted mito^{4x}-GCaMP6f and the outer membrane-targeted OMM-jRCaMP1b signal (A) in response to a given stimulus in mitochondria of "spiking" HEK cells (B) and neuronal axons (C) (n = 6–49 cells). Responses in "spiking" HEK cells were binned across OMM responses for ease of comparison with neurons.

(B and C) Averaged traces of matrix (green) Ca^{2+} fluxes in "spiking" HEK cells (n = 29 cells) (B) and neuronal axons (n = 49 cells) (C) in response to 20 AP at 20 Hz in neurons and the equivalent Ca^{2+} increase in the OMM of HEK cells, measured by quantifying OMM Ca^{2+} signals (red) in both cell types (traces not shown for clarity, but average OMM peak response is denoted with a red dashed line). Experiments were performed in the presence of glucose. Error bars indicate SEM. **p < 0.01, ****p < 0.0001, Mann-Whitney U test.

Higher Ca^{2+} Concentrations Are Needed to Trigger Mitochondrial Ca^{2+} Uptake in Non-neuronal Cells Compared to Nerve Terminals

The finding that axonal mitochondria are freed from the constraints of relying on ER Ca^{2+} to activate MCU implies either that axonal mitochondria normally occupy a privileged location close to sites of plasma-membrane Ca^{2+} entry or that the machinery associated with MCU activation is specifically tuned to operate with lower Ca^{2+} concentrations in axons. To distinguish between these two scenarios, we developed a novel approach that allowed us to compare the Ca^{2+} signals needed on the outer mitochondrial membrane (OMM) to trigger Ca^{2+} uptake into the mitochondrial matrix in a non-neuronal cell versus a neuronal axon. To measure OMM Ca^{2+} signals, we fused the genetically encoded red-shifted Ca^{2+} indicator jRCaMP1b (Dana et al., 2016) to a portion of the OMM protein TOM20 and expressed this construct in neurons. Ca^{2+} influx in axons can be robustly stimulated and controlled by varying AP firing at a fixed extracellular Ca^{2+} concentration. Over many experiments across axons of many individual neurons, we compared the mitochondrial matrix GCaMP6f signal for a given stimulus condition with the OMM jRCaMP1b signal for the same stimulus condition. We then correlated the matrix Ca^{2+} signal obtained for a given stimulus with the OMM signal for the same stimulus. These experiments show that axonal mitochondrial Ca^{2+} uptake appears non-linear. With minimal Ca^{2+} entry (e.g., a 3-AP stimulus) that generates a robust OMM signal, the matrix signal is negligible (Figure 4A). However, increasing the OMM signal by ~2.5-fold led to a greater than 10-fold increase in the matrix signal (Figures 4A and 4C).

In order to determine the sensitivity of non-neuronal mitochondria, we developed a novel approach to allow us to reproducibly induce transient changes in cytosolic Ca^{2+} that do not depend on ER function in human embryonic kidney (HEK) cells. We made use of the development of "spiking" HEK cells (Park et al., 2013), which express $Na_v1.3$ and $K_{IR}2.1$. These cells show a reproducible and transient membrane depolarization in response to brief electrical field stimulation, which we confirmed using the fluorescent voltage sensor Ace-mNeon (Gong et al., 2015) (Figures S2A and S2B). We transiently transfected these cells with our mitochondrial OMM and matrix reporters (see STAR Methods), along with plasmids encoding the three genes necessary for the surface expression of a $Ca_v2.1$ voltage-gated Ca^{2+} channel (α1b, $\alpha2\delta1$, and $\beta1$). A brief field potential stimulus in these cells leads to a very robust and transient influx of Ca^{2+} across the plasma membrane without causing ER Ca^{2+} release (Figure S2C). By varying the concentration of extracellular Ca^{2+}, we could vary the size of the OMM signal and determine the correlation of mitochondrial Ca^{2+} uptake with OMM Ca^{2+} in these non-neuronal cells. These experiments showed that, unlike neurons, mitochondria in HEK cells remained unresponsive over a much wider range of OMM Ca^{2+} signals (Figures 4A and 4B). The transition from minimal Ca^{2+} uptake to robust Ca^{2+} uptake appeared, as with neuronal mitochondria, to be non-linear, where a doubling of OMM Ca^{2+} signal (from a $\Delta F/F$ of 0.42 to 0.84) led to a greater than 10-fold increase in the matrix Ca^{2+} signal. However, the apparent set point for this transition was ~3-fold higher in HEK cells compared to neurons. These experiments indicate that the likely reason axonal mitochondria do not depend on ER function is that their machinery for mitochondrial Ca^{2+} uptake is tuned to be responsive to smaller OMM Ca^{2+} signals to facilitate MCU opening during modest AP firing.

MICU3 Shifts the Ca^{2+} Sensitivity of Presynaptic Mitochondrial Ca^{2+} Uptake

The experiments above demonstrate that axonal mitochondria have a significantly different Ca^{2+} sensitivity for activating mitochondrial Ca^{2+} uptake than non-neuronal mitochondria. The Ca^{2+}-dependent activation of MCU is conferred by a set of EF-hand-containing regulatory proteins, MICUs, that assemble around MCU in the mitochondrial intermembrane space (Marchi and Pinton, 2014). In most tissues, this is conveyed by MICU1 and MICU2, where it is thought that MICU1 is responsible for keeping MCU in a closed state (Mallilankaraman et al., 2012), and MICU2 allows Ca^{2+}-dependent MCU opening (Patron et al., 2014). MICU3 is a brain-specific isoform that is exclusively expressed in neurons (Plovanich et al., 2013) and was recently shown to enhance mitochondrial Ca^{2+} uptake when expressed in non-neuronal cells (Patron et al., 2019). We reasoned that MICU3 might be responsible for the lower threshold of Ca^{2+}-driven MCU activated in axonal mitochondria. To test this

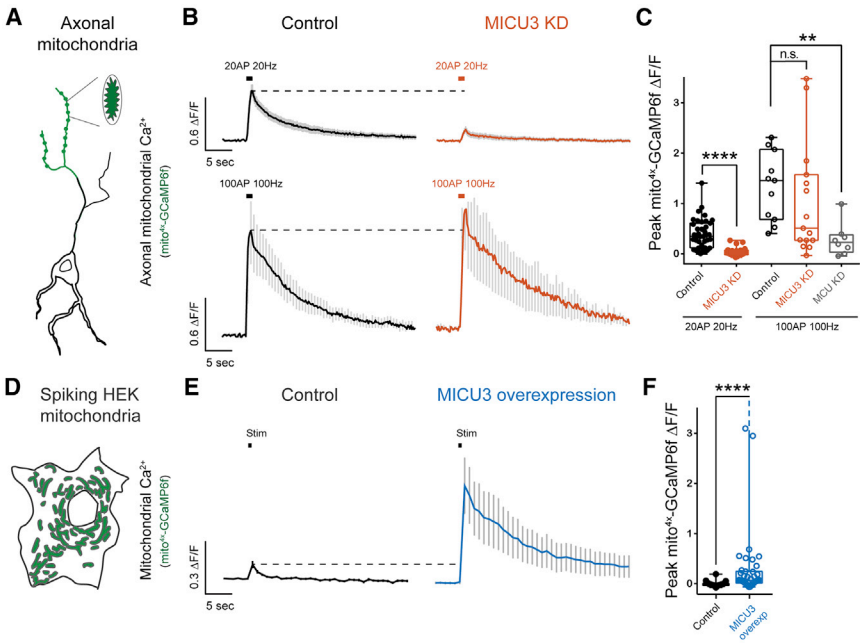

Figure 5. MICU3 Shifts the Ca^{2+} Sensitivity of Presynaptic Mitochondrial Ca^{2+} Uptake

(A–C) Average traces of mito^{4x}-GCaMP6f (B) in neuronal axons (schematic in A) stimulated with 20 AP at 20 Hz (B, top panel) or 100 AP at 100 Hz (B, bottom panel) in control and MICU3 KD neurons. (C) Peak mito^{4x}-GCaMP6f ΔF/F following stimulation. n = 8–39 cells. Average ΔF/F ± SEM: control (20 AP at 20 Hz) (same as in Figures 2A and 2B), 0.41 ± 0.05; MICU3 KD (20 AP at 20 Hz), 0.04 ± 0.02; control (100 AP at 100 Hz), 1.33 ± 0.20; MICU3 (100 AP at 100 Hz), 1.04 ± 0.29; MCU KD (100 AP at 100 Hz), 0.28 ± 0.11.

(D–F) Average traces of mito^{4x}-GCaMP6f (E) in control and MICU3-overexpressing "spiking" HEK cells (schematic in D) stimulated for 10 ms. To facilitate comparison, only HEK cells whose OMM Ca^{2+} signals are equivalent to neurons stimulated with 20 AP at 20 Hz are plotted. (F) Peak mito^{4x}-GCaMP6f ΔF/F following stimulation. n = 34–43 cells. Average ΔF/F ± SEM: control, 0.03 ± 0.01; MICU3 overexpression, 0.4 ± 0.13.

Error bars indicate SEM. $^{**}p < 0.01$, $^{****}p < 0.0001$, n.s., not statistically significant Mann-Whitney U test. The box-whisker plot represents median (line), 25th–75th percentile (box), and min–max (whisker).

idea, we used a shRNA-mediated knockdown of MICU3 (Figure S3A) and examined axonal mitochondrial Ca^{2+} uptake in dissociated primary hippocampal neurons using mito^{4x}-GCaMP6f. Although loss of MICU3 led to significant suppression of mitochondrial Ca^{2+} uptake (Figures 5A–5C) for our standard conditions (20 AP at 20 Hz firing) without changing the resting mitochondrial Ca^{2+} level (Figure S3B), it did not prevent mitochondrial Ca^{2+} uptake for more intense stimuli (100 AP at 100 Hz, which is outside the likely physiological range for hippocampal neurons) (Figures 5A–5C). Such stimuli did not saturate our mitochondrial Ca^{2+} sensor (Figures S3C and S3D). The suppression of mitochondrial Ca^{2+} uptake was reversed by re-expression of a shRNA-insensitive variant of MICU3 (Figure S3E). The inability to suppress mitochondrial Ca^{2+} uptake with more intense stimuli after loss of MICU3 was in contrast to loss of MCU, which suppressed mitochondrial Ca^{2+} uptake for both types of stimuli (Figures 2A, 2B, and 5C). Because more intense stimuli lead to greater elevations in cytoplasmic Ca^{2+} (Figures S3F and S3G), we conclude that without MICU3, axonal mitochondria require higher Ca^{2+} to trigger Ca^{2+} uptake like that measured in non-neuronal cells (Figures S3G and 4A). Conversely, expression of MICU3 in "spiking" HEK cells shifted the mitochondria to a much more Ca^{2+}-sensitive state and were now similar to mitochondria in neuronal axons (Figures 5D–5F). Thus, MICU3 expression is sufficient to significantly switch the ability of mitochondria to respond to smaller cytosolic Ca^{2+} elevations.

MICU3 Is Required for Feedforward Regulation of ATP Production in Nerve Terminals

We showed that Ca^{2+} uptake in axonal mitochondria is a critical aspect of a feedforward-mediated regulation of ATP synthesis, which, under oxidative conditions, is critical for presynaptic function (Figure 2). We therefore examined whether MICU3-enhanced Ca^{2+} sensitivity of Ca^{2+} uptake in neuronal mitochondria contributes to metabolic regulation at nerve terminals. Measurements of ATP at nerve terminals showed that when MICU3 expression is suppressed, ATP levels cannot be sustained during 60 s of 10 Hz AP firing (Figures 6A and 6B), similar to what was found in neurons lacking MCU. This inability to sustain ATP synthesis resulted in slowing of SV recycling as probed with vGLUT1-pH (Figures 6C and 6D). Switching the fuel source to glucose, however, fully restored SV recycling kinetics, indicating, as with loss of MCU, that chronic loss of MICU3 does not lead to pleiotropic impairment of presynaptic machinery. These findings demonstrate that MICU3 is critical in neurons to allow the transition from glycolytic to oxidative metabolism in supporting activity-driven ATP production.

DISCUSSION

The metabolic vulnerability of the brain underpins the importance of understanding how fuel is delivered, how brain metabolism is regulated, and the efficiency with which neuronal processes utilize metabolic products, including ATP. Inevitably, any disruption in these metabolic processes could lead to neuronal dysfunction and cognitive decline. The processes of SV cycling and maintaining ionic homeostasis during neuronal firing come at steep metabolic costs and require ATP production to adjust according to demand. We have previously shown that ATP levels remain unperturbed at nerve terminals when going from a resting state to constant AP firing despite increased energy consumption (Rangaraju et al., 2014) because of concomitant upregulation of presynaptic ATP production.

Although glycolytic ATP synthesis is stimulated during activity (Ashrafi and Ryan, 2017), the ATP produced solely by glycolysis

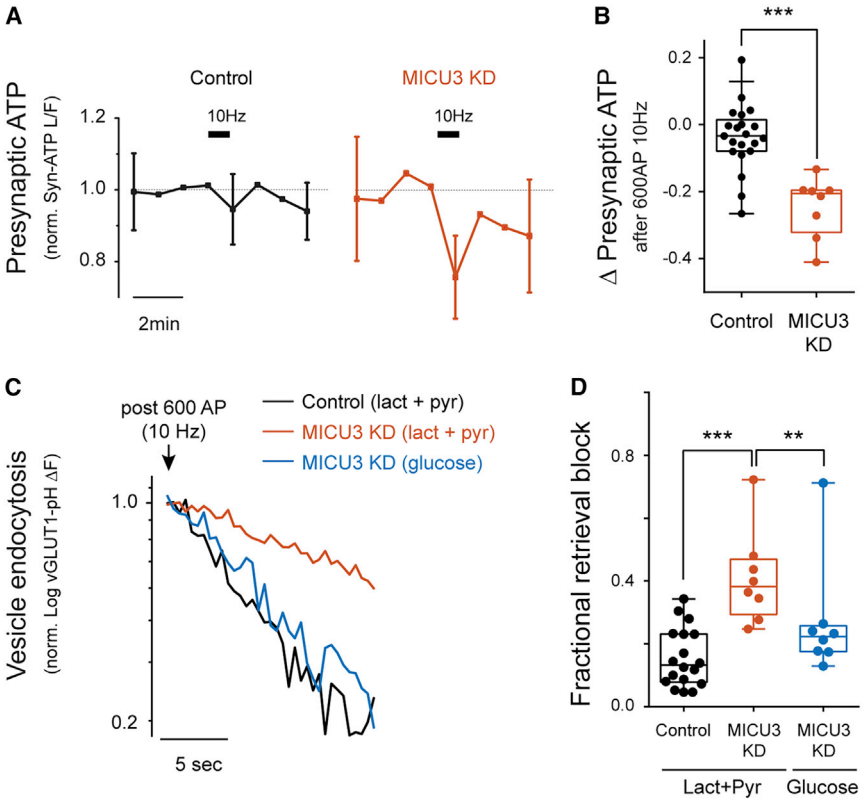

Figure 6. MICU3 Is Required for Feedforward Regulation of ATP Production in Nerve Terminals

(A and B) Normalized presynaptic ATP traces (A) in control and MICU3 KD neurons stimulated with 600 AP at 10 Hz supplied with lactate and pyruvate. The gray dashed line represents the normalized ATP value of 1. (B) Change in normalized ATP levels immediately after stimulation. n = 8–21 cells. Average change in ATP; control (same as in Figures 2C and 2D), −0.04 ± 0.02; MICU3 KD, −0.25 ± 0.03. ***p < 0.001, Mann-Whitney U test.

(C and D) Sample semi-log plot of vGLUT1-pH traces (C) following stimulation with 600 AP at 10 Hz in control and MICU3 KD neurons supplied with lactate and pyruvate or glucose. (D) Fractional retrieval block as described in STAR Methods. n = 8–21 cells. Average retrieval block ± SEM: Control (same as in Figures 2E and 2F), 0.16 ± 0.02; MICU3 KD (lact+pyr), 0.41 ± 0.05; MICU3 KD (glucose), 0.27 ± 0.07.

Error bars indicate SEM. **p < 0.01, ***p < 0.001, Kruskal-Wallis H Test. The box-whisker plot represents median (line), 25th–75th percentile (box), and min–max (whisker).

may be insufficient to support function under physiological concentrations of brain glucose, which is significantly lower than that of the blood (McNay and Gold, 1999). Additionally, it has long been argued that lactate derived from peri-synaptic astrocytes is the main fuel sustaining synapse function (Pellerin et al., 1998). This intrinsic variability in how synapses are fueled implies that they likely upregulate ATP synthesis in a fuel-dependent fashion. Thus, proper regulation of ATP production in response to activity requires distinct mechanisms suited for different metabolic conditions. We show here that nerve terminals are metabolically flexible and can carry out vesicle recycling when dispensing entirely with glycolysis (Figure 1C), in agreement with previous reports (Pathak et al., 2015). Measurements of ATP concentration during activity under these conditions indicate that, as with glycolysis, mitochondrial ATP production is also upregulated by AP firing. Such metabolic flexibility is notable given the observation that only about 50% of hippocampal *en passant* boutons contain mitochondria (Kang et al., 2008) and therefore have immediate access to mitochondrially derived ATP. At present, it is unclear whether relying on ATP produced from a neighboring bouton's mitochondria will impose severe constraints on performance. Our previous work indicates that dependence on new ATP synthesis kicks in during repetitive AP firing after a few seconds. Over this timescale, an average inter-bouton distance of ~3 μm (Smith et al., 2016) is likely close enough to allow for the diffusion of newly synthesized ATP, as previously reported (Pathak et al., 2015).

Although mitochondrial Ca^{2+} uptake has long been proposed to modulate the capacity of mitochondria to produce ATP, to our knowledge, the experiments in Figure 2D are the first to demonstrate that, in intact cells, mitochondrial Ca^{2+} uptake is critical for metabolic support. Here, Ca^{2+} is used as a feedforward signal serving as a surrogate for the increased energetic demands associated with Ca^{2+} entry from the plasma membrane. This system compliments but differs from the regulation of glycolysis, where a feedback mechanism, based on AMPK activation (and therefore reflecting the detection of a transient energy deficit), regulates glucose uptake. The downstream mechanisms by which mitochondrial Ca^{2+} uptake drives ATP synthesis have not been explored in neurons.

In non-neuronal cells, mitochondrial Ca^{2+} uptake has been shown to take place where mitochondria form sites of close apposition with the ER (Rizzuto et al., 1993, 1998). This spatial relationship is thought to allow MCU activation to have a high threshold with respect to Ca^{2+} concentration, as upon ER Ca^{2+} release, the outer and inner mitochondrial membranes would experience local micro-domains of high Ca^{2+}, enabling MCU to open. Mitochondria-ER contacts have been identified in most cell types examined, including neurons (Wu et al., 2017). Presumably, if nerve terminals relied on ER Ca^{2+} release to trigger mitochondrial Ca^{2+} uptake, an initial Ca^{2+} influx from the plasma membrane (through voltage-gated Ca^{2+} channels) would need to trigger Ca^{2+} release from the ER. By silencing axonal ER Ca^{2+} fluxes (de Juan-Sanz et al., 2017), we demonstrated that axonal mitochondrial Ca^{2+} uptake during AP firing is completely independent of the ER's ability to flux Ca^{2+}. Given the long-held view that mitochondrial Ca^{2+} uptake is tightly controlled by its intimate spatial proximity with the ER, two possibilities arose: first, in axons, mitochondria are positioned very close to voltage-gated Ca^{2+} channels on the plasma membrane such

that they always sense high Ca^{2+} during activity; or second, the molecular machinery for mitochondrial Ca^{2+} uptake in axonal mitochondria is different from other tissues. Our quantitative measurement of the cytoplasmic signals that can drive mitochondrial Ca^{2+} uptake (Figure 4) demonstrated that axonal mitochondria have a lower threshold for triggering mitochondrial Ca^{2+} uptake than mitochondria in non-neuronal cells and therefore do not need to be positioned close to other Ca^{2+} sources. However, the molecular machinery controlling mitochondrial Ca^{2+} uptake in other tissues appears to be different from that in neurons. It is possible that in other subcellular regions of a neuron, mitochondrial Ca^{2+} uptake has a greater dependence on Ca^{2+} release from the ER, as has been reported for mitochondrial Ca^{2+} uptake in dendrites (Hirabayashi et al., 2017). Although it has been widely assumed that the physical contacts between the ER and mitochondria facilitate mitochondrial Ca^{2+} uptake, our data imply that these contacts in axons likely serve different roles, for example, regulating lipid homeostasis.

It is interesting to note than even across non-neuronal tissues, MCU-based Ca^{2+} uptake activity is highly variable (Fieni et al., 2012). This may be, in part, because of differential tissue expression of the MCU regulators, MICUs. Unlike MICU1 and MICU2, MICU3 is exclusively expressed in the brain and enhances MCU activity in non-neuronal cells. To our knowledge, our studies are the first to uncover the physiological significance of the neuronal-specific expression of MICU3. We reason that the MICU3-mediated tuning of mitochondrial Ca^{2+} uptake is critical for the coordination of ATP synthesis and consumption in firing nerve terminals. However, mitochondrial Ca^{2+} uptake likely conveys risks as well, as overloading Ca^{2+} in the mitochondrial matrix is thought to facilitate the permeability transition of the inner membrane, in turn leading to necro-apoptotic cascades (Krieger and Duchen, 2002). Whether neuronal mitochondria have specific mechanisms at work to mitigate this risk is an important question that requires further investigation. Given the metabolic vulnerability of the nervous system, our identification of the molecular machinery for activity-dependent regulation of mitochondrial ATP, future studies should strive to determine whether mutations in the components of the MCU complex give rise to neurodegeneration in human patients.

It is interesting to note that in addition to glucose and lactate, the brain can also, under some conditions, be fueled by ketone bodies. How this fuel source is utilized and how its combustion is regulated are not completely understood (Lutas and Yellen, 2013). Given that strict ketogenic diets are used to curtail certain forms of intractable epilepsies (Neal et al., 2008), in the future, it will be interesting to dissect how regulation of ketone usage differs from other fuel sources at the synapse and whether any regulatory differences impact synapse function and cognitive performance.

This metabolic plasticity of neurons provides a plausible explanation to why genetic or pharmacological manipulation of metabolic pathways often fails to exhibit dramatic cognitive phenotypes. For example, despite its crucial role in the regulation of presynaptic glycolysis, Glut4 knockout mice survive (Abel et al., 1999) and have not been reported to have gross cognitive impairment. Similarly, inhibition of pyruvate import into neuronal mitochondria does not impair gross ATP production or survival and merely results in metabolic reprogramming (Divakaruni et al., 2017). Such robust metabolic plasticity in the mammalian brain most likely serves to ensure that cognitive performance is faithfully maintained in the face of changing nutrient availability.

STAR★METHODS

Detailed methods are provided in the online version of this paper and include the following:

- KEY RESOURCES TABLE
- LEAD CONTACT AND MATERIALS AVAILABILITY
- EXPERIMENTAL MODEL AND SUBJECT DETAILS
  - Animals
  - Primary Neuronal Culture
  - Culture and transfection of "Spiking" HEK293 cells
- METHOD DETAILS
  - Plasmid Constructs
  - Lentiviral Production and Application
  - Live Imaging of Neurons
  - Live Imaging of "Spiking" HEK293 cells
  - RNA Isolation and Quantitative PCR
  - Experimental design
- QUANTIFICATION AND STATISTICAL ANALYSIS
  - Image Analysis and Statistics
  - Quantification of Synaptic Vesicle Fractional Retrieval Block
  - Analysis of "Spiking" HEK293 Cells
  - Mitochondrial Ca^{2+} measurements using mito^{4x}-GCaMP6f
  - Resting mitochondrial Ca^{2+} estimates using mito^{4x}-GCaMP6f
  - Mitochondrial pH measurements
- DATA AND CODE AVAILABILITY

SUPPLEMENTAL INFORMATION

Supplemental Information can be found online at https://doi.org/10.1016/j.neuron.2019.11.020.

ACKNOWLEDGMENTS

We thank members of the Ryan lab for frequent discussions about this work and Adam Cohen (Harvard University) for generously providing the "spiking" HEK cells. This work was supported by the NIH (NS036942 and MH085783 to T.A.R.).

AUTHOR CONTRIBUTIONS

Conceptualization, G.A., J.d.J.-S., and T.A.R.; Investigation, G.A., J.d.J.-S., and R.J.F.; Writing – Original Draft, G.A., J.d.J.-S., and T.A.R.; Writing – Review & Editing, G.A., J.d.J.-S., R.J.F., and T.A.R.; Visualization, G.A., J.d.J.-S., and R.J.F.; Funding Acquisition, T.A.R.; Supervision, T.A.R.

DECLARATION OF INTERESTS

The authors declare no competing interests.

Received: July 19, 2019
Revised: October 16, 2019
Accepted: November 12, 2019
Published: December 17, 2019

REFERENCES

Abel, E.D., Kaulbach, H.C., Tian, R., Hopkins, J.C., Duffy, J., Doetschman, T., Minnemann, T., Boers, M.E., Hadro, E., Oberste-Berghaus, C., et al. (1999). Cardiac hypertrophy with preserved contractile function after selective deletion of GLUT4 from the heart. J. Clin. Invest. *104*, 1703–1714.

Armbruster, M., and Ryan, T.A. (2011). Synaptic vesicle retrieval time is a cell-wide rather than individual-synapse property. Nat. Neurosci. *14*, 824–826.

Ashrafi, G., and Ryan, T.A. (2017). Glucose metabolism in nerve terminals. Curr. Opin. Neurobiol. *45*, 156–161.

Ashrafi, G., Wu, Z., Farrell, R.J., and Ryan, T.A. (2017). GLUT4 Mobilization Supports Energetic Demands of Active Synapses. Neuron *93*, 606–615.e3.

Balaji, J., and Ryan, T.A. (2007). Single-vesicle imaging reveals that synaptic vesicle exocytosis and endocytosis are coupled by a single stochastic mode. Proc. Natl. Acad. Sci. USA *104*, 20576–20581.

Baughman, J.M., Perocchi, F., Girgis, H.S., Plovanich, M., Belcher-Timme, C.A., Sancak, Y., Bao, X.R., Strittmatter, L., Goldberger, O., Bogorad, R.L., et al. (2011). Integrative genomics identifies MCU as an essential component of the mitochondrial calcium uniporter. Nature *476*, 341–345.

Campeau, E., Ruhl, V.E., Rodier, F., Smith, C.L., Rahmberg, B.L., Fuss, J.O., Campisi, J., Yaswen, P., Cooper, P.K., and Kaufman, P.D. (2009). A versatile viral system for expression and depletion of proteins in mammalian cells. PLoS ONE *4*, e6529.

Chen, T.W., Wardill, T.J., Sun, Y., Pulver, S.R., Renninger, S.L., Baohan, A., Schreiter, E.R., Kerr, R.A., Orger, M.B., Jayaraman, V., et al. (2013). Ultrasensitive fluorescent proteins for imaging neuronal activity. Nature *499*, 295–300.

Cohen, L.D., Zuchman, R., Sorokina, O., Müller, A., Dieterich, D.C., Armstrong, J.D., Ziv, T., and Ziv, N.E. (2013). Metabolic turnover of synaptic proteins: kinetics, interdependencies and implications for synaptic maintenance. PLoS ONE *8*, e63191.

Dana, H., Mohar, B., Sun, Y., Narayan, S., Gordus, A., Hasseman, J.P., Tsegaye, G., Holt, G.T., Hu, A., Walpita, D., et al. (2016). Sensitive red protein calcium indicators for imaging neural activity. eLife *5*, e12727.

de Juan-Sanz, J., Holt, G.T., Schreiter, E.R., de Juan, F., Kim, D.S., and Ryan, T.A. (2017). Axonal Endoplasmic Reticulum Ca^{2+} Content Controls Release Probability in CNS Nerve Terminals. Neuron *93*, 867–881.e6.

De Stefani, D., Raffaello, A., Teardo, E., Szabò, I., and Rizzuto, R. (2011). A forty-kilodalton protein of the inner membrane is the mitochondrial calcium uniporter. Nature *476*, 336–340.

Divakaruni, A.S., Wallace, M., Buren, C., Martyniuk, K., Andreyev, A.Y., Li, E., Fields, J.A., Cordes, T., Reynolds, I.J., Bloodgood, B.L., et al. (2017). Inhibition of the mitochondrial pyruvate carrier protects from excitotoxic neuronal death. J. Cell Biol. *216*, 1091–1105.

Emptage, N.J., Reid, C.A., and Fine, A. (2001). Calcium stores in hippocampal synaptic boutons mediate short-term plasticity, store-operated Ca2+ entry, and spontaneous transmitter release. Neuron *29*, 197–208.

Enomoto, M., Bunge, M.B., and Tsoulfas, P. (2013). A multifunctional neurotrophin with reduced affinity to p75NTR enhances transplanted Schwann cell survival and axon growth after spinal cord injury. Exp. Neurol. *248*, 170–182.

Fieni, F., Lee, S.B., Jan, Y.N., and Kirichok, Y. (2012). Activity of the mitochondrial calcium uniporter varies greatly between tissues. Nat. Commun. *3*, 1317.

Glancy, B., and Balaban, R.S. (2012). Role of mitochondrial Ca2+ in the regulation of cellular energetics. Biochemistry *51*, 2959–2973.

Gong, Y., Huang, C., Li, J.Z., Grewe, B.F., Zhang, Y., Eismann, S., and Schnitzer, M.J. (2015). High-speed recording of neural spikes in awake mice and flies with a fluorescent voltage sensor. Science *350*, 1361–1366.

Greotti, E., Fortunati, I., Pendin, D., Ferrante, C., Galla, L., Zentilin, L., Giacca, M., Kaludercic, N., Di Sante, M., Mariotti, L., et al. (2019). mCerulean3-Based Cameleon Sensor to Explore Mitochondrial Ca. iScience *19*, 161.

Gunter, T.E., Gunter, K.K., Sheu, S.S., and Gavin, C.E. (1994). Mitochondrial calcium transport: physiological and pathological relevance. Am. J. Physiol. *267*, C313–C339.

Heineman, F.W., and Balaban, R.S. (1990). Phosphorus-31 nuclear magnetic resonance analysis of transient changes of canine myocardial metabolism in vivo. J. Clin. Invest. *85*, 843–852.

Heo, S., Diering, G.H., Na, C.H., Nirujogi, R.S., Bachman, J.L., Pandey, A., and Huganir, R.L. (2018). Identification of long-lived synaptic proteins by proteomic analysis of synaptosome protein turnover. Proc. Natl. Acad. Sci. USA *115*, E3827–E3836.

Hirabayashi, Y., Kwon, S.K., Paek, H., Pernice, W.M., Paul, M.A., Lee, J., Erfani, P., Raczkowski, A., Petrey, D.S., Pon, L.A., et al. (2017). ER-mitochondria tethering by PDZD8 regulates Ca. Science *358*, 623–630.

Hoppa, M.B., Lana, B., Margas, W., Dolphin, A.C., and Ryan, T.A. (2012). $\alpha 2\delta$ expression sets presynaptic calcium channel abundance and release probability. Nature *486*, 122–125.

Ikemoto, A., Bole, D.G., and Ueda, T. (2003). Glycolysis and glutamate accumulation into synaptic vesicles. Role of glyceraldehyde phosphate dehydrogenase and 3-phosphoglycerate kinase. J. Biol. Chem. *278*, 5929–5940.

Kanaji, S., Iwahashi, J., Kida, Y., Sakaguchi, M., and Mihara, K. (2000). Characterization of the signal that directs Tom20 to the mitochondrial outer membrane. J. Cell Biol. *151*, 277–288.

Kang, J.S., Tian, J.H., Pan, P.Y., Zald, P., Li, C., Deng, C., and Sheng, Z.H. (2008). Docking of axonal mitochondria by syntaphilin controls their mobility and affects short-term facilitation. Cell *132*, 137–148.

Kingston, R.E., Chen, C.A., and Okayama, H. (2001). Calcium phosphate transfection. Curr Protoc Immunol *Chapter 10*. Unit 10.13.

Knull, H.R., and Fillmore, S.J. (1985). Glycolytic enzyme levels in synaptosomes. Comp. Biochem. Physiol. B *81*, 349–351.

Krieger, C., and Duchen, M.R. (2002). Mitochondria, Ca2+ and neurodegenerative disease. Eur. J. Pharmacol. *447*, 177–188.

Liang, Y., Yuan, L.L., Johnston, D., and Gray, R. (2002). Calcium signaling at single mossy fiber presynaptic terminals in the rat hippocampus. J. Neurophysiol. *87*, 1132–1137.

Lutas, A., and Yellen, G. (2013). The ketogenic diet: metabolic influences on brain excitability and epilepsy. Trends Neurosci. *36*, 32–40.

Mallilankaraman, K., Doonan, P., Cárdenas, C., Chandramoorthy, H.C., Müller, M., Miller, R., Hoffman, N.E., Gandhirajan, R.K., Molgó, J., Birnbaum, M.J., et al. (2012). MICU1 is an essential gatekeeper for MCU-mediated mitochondrial Ca(2+) uptake that regulates cell survival. Cell *151*, 630–644.

Marchi, S., and Pinton, P. (2014). The mitochondrial calcium uniporter complex: molecular components, structure and physiopathological implications. J. Physiol. *592*, 829–839.

McNay, E.C., and Gold, P.E. (1999). Extracellular glucose concentrations in the rat hippocampus measured by zero-net-flux: effects of microdialysis flow rate, strain, and age. J. Neurochem. *72*, 785–790.

Moffat, J., Grueneberg, D.A., Yang, X., Kim, S.Y., Kloepfer, A.M., Hinkle, G., Piqani, B., Eisenhaure, T.M., Luo, B., Grenier, J.K., et al. (2006). A lentiviral RNAi library for human and mouse genes applied to an arrayed viral high-content screen. Cell *124*, 1283–1298.

Neal, E.G., Chaffe, H., Schwartz, R.H., Lawson, M.S., Edwards, N., Fitzsimmons, G., Whitney, A., and Cross, J.H. (2008). The ketogenic diet for the treatment of childhood epilepsy: a randomised controlled trial. Lancet Neurol. *7*, 500–506.

Pan, X., Liu, J., Nguyen, T., Liu, C., Sun, J., Teng, Y., Fergusson, M.M., Rovira, I.I., Allen, M., Springer, D.A., et al. (2013). The physiological role of mitochondrial calcium revealed by mice lacking the mitochondrial calcium uniporter. Nat. Cell Biol. *15*, 1464–1472.

Park, J., Werley, C.A., Venkatachalam, V., Kralj, J.M., Dib-Hajj, S.D., Waxman, S.G., and Cohen, A.E. (2013). Screening fluorescent voltage indicators with spontaneously spiking HEK cells. PLoS ONE *8*, e85221.

Pathak, D., Shields, L.Y., Mendelsohn, B.A., Haddad, D., Lin, W., Gerencser, A.A., Kim, H., Brand, M.D., Edwards, R.H., and Nakamura, K. (2015). The role of mitochondrially derived ATP in synaptic vesicle recycling. J. Biol. Chem. *290*, 22325–22336.

Patron, M., Checchetto, V., Raffaello, A., Teardo, E., Vecellio Reane, D., Mantoan, M., Granatiero, V., Szabò, I., De Stefani, D., and Rizzuto, R. (2014). MICU1 and MICU2 finely tune the mitochondrial Ca2+ uniporter by exerting opposite effects on MCU activity. Mol. Cell *53*, 726–737.

Patron, M., Granatiero, V., Espino, J., Rizzuto, R., and De Stefani, D. (2019). MICU3 is a tissue-specific enhancer of mitochondrial calcium uptake. Cell Death Differ. *26*, 179–195.

Pellerin, L., Pellegri, G., Bittar, P.G., Charnay, Y., Bouras, C., Martin, J.L., Stella, N., and Magistretti, P.J. (1998). Evidence supporting the existence of an activity-dependent astrocyte-neuron lactate shuttle. Dev. Neurosci. *20*, 291–299.

Plovanich, M., Bogorad, R.L., Sancak, Y., Kamer, K.J., Strittmatter, L., Li, A.A., Girgis, H.S., Kuchimanchi, S., De Groot, J., Speciner, L., et al. (2013). MICU2, a paralog of MICU1, resides within the mitochondrial uniporter complex to regulate calcium handling. PLoS ONE *8*, e55785.

Posner, J.B., Saper, C.B., Schiff, N.D., Plum, F., 2007. In: Plum and Posner's Diagnosis of Stupor and Coma, 4th ed. Oxford University Press, pp. 179–205.

Qiu, J., Tan, Y.W., Hagenston, A.M., Martel, M.A., Kneisel, N., Skehel, P.A., Wyllie, D.J., Bading, H., and Hardingham, G.E. (2013). Mitochondrial calcium uniporter Mcu controls excitotoxicity and is transcriptionally repressed by neuroprotective nuclear calcium signals. Nat. Commun. *4*, 2034.

Rangaraju, V., Calloway, N., and Ryan, T.A. (2014). Activity-driven local ATP synthesis is required for synaptic function. Cell *156*, 825–835.

Rizzuto, R., Brini, M., Murgia, M., and Pozzan, T. (1993). Microdomains with high Ca2+ close to IP3-sensitive channels that are sensed by neighboring mitochondria. Science *262*, 744–747.

Rizzuto, R., Pinton, P., Carrington, W., Fay, F.S., Fogarty, K.E., Lifshitz, L.M., Tuft, R.A., and Pozzan, T. (1998). Close contacts with the endoplasmic reticulum as determinants of mitochondrial Ca2+ responses. Science *280*, 1763–1766.

Ryan, T.A. (1999). Inhibitors of myosin light chain kinase block synaptic vesicle pool mobilization during action potential firing. J. Neurosci. *19*, 1317–1323.

Schönfeld, P., and Reiser, G. (2013). Why does brain metabolism not favor burning of fatty acids to provide energy? Reflections on disadvantages of the use of free fatty acids as fuel for brain. J. Cereb. Blood Flow Metab. *33*, 1493–1499.

Seehusen, D.A., Reeves, M.M., and Fomin, D.A. (2003). Cerebrospinal fluid analysis. Am. Fam. Physician *68*, 1103–1108.

Smith, H.L., Bourne, J.N., Cao, G., Chirillo, M.A., Ostroff, L.E., Watson, D.J., and Harris, K.M. (2016). Mitochondrial support of persistent presynaptic vesicle mobilization with age-dependent synaptic growth after LTP. eLife *5*, e15275.

Sparagna, G.C., Gunter, K.K., and Gunter, T.E. (1994). A system for producing and monitoring in vitro calcium pulses similar to those observed in vivo. Anal. Biochem. *219*, 96–103.

Vannucci, R.C., and Vannucci, S.J. (2000). Glucose metabolism in the developing brain. Semin. Perinatol. *24*, 107–115.

Venkatachalam, V., and Cohen, A.E. (2014). Imaging GFP-based reporters in neurons with multiwavelength optogenetic control. Biophys. J. *107*, 1554–1563.

Voglmaier, S.M., Kam, K., Yang, H., Fortin, D.L., Hua, Z., Nicoll, R.A., and Edwards, R.H. (2006). Distinct endocytic pathways control the rate and extent of synaptic vesicle protein recycling. Neuron *51*, 71–84.

Wu, Y., Whiteus, C., Xu, C.S., Hayworth, K.J., Weinberg, R.J., Hess, H.F., and De Camilli, P. (2017). Contacts between the endoplasmic reticulum and other membranes in neurons. Proc. Natl. Acad. Sci. USA *114*, E4859–E4867.

Yan, H., Pablo, J.L., and Pitt, G.S. (2013). FGF14 regulates presynaptic Ca2+ channels and synaptic transmission. Cell Rep. *4*, 66–75.

Yellen, G. (2018). Fueling thought: Management of glycolysis and oxidative phosphorylation in neuronal metabolism. J. Cell Biol. *217*, 2235–2246.

STAR★METHODS

KEY RESOURCES TABLE

REAGENT or RESOURCE	SOURCE	IDENTIFIER
Chemicals, Peptides, and Recombinant Proteins		
Cyclopiazonic Acid	Alomone	CAT#: C-750
Ionomycin	Alomone	CAT#: I-700
Oligomycin A	Enzo Life Sciences	CAT#: ALX-380-037
Chloroform	Sigma	CAT#: 288306
TRIzol	Thermo Fisher	CAT#: 15596026
Critical Commercial Assays		
QuickChange site-directed mutagenesis kit	Agilent Technologies	CAT#: 210518
RNeasy Mini Kit	QIAGEN	CAT#: 74104
SuperScript IV VILO Master Mix with ezDNase Enzyme	Thermo Fisher	CAT#: 11766050
TaqMan Fast Advanced Master Mix	Thermo Fisher	CAT#: 4444557
Actb TaqMan Gene Expression Assay	Thermo Fisher	CAT#: 4448484 Assay ID: Rn00667869_m1
MCU TaqMan Gene Expression Assay	Thermo Fisher	CAT#: 4448892 Assay ID: Rn01433739_m1
MICU3 TaqMan Gene Expression Assay	Thermo Fisher	CAT#: 4448892 Assay ID: Rn01487906_m1
Lenti-X qRT-PCR Titration Kit	Takara	CAT#: 631235
Experimental Models: Cell Lines		
Spiking HEK293 Cells	Park et al., 2013	N/A
Experimental Models: Organisms/Strains		
Sprague-Dawley Rat	Charles River	Strain code: 400, RRID: RGD_734476
Recombinant DNA for neurons and HEK cells		
vGLUT1-pHluorin	Voglmaier et al., 2006	N/A
ER-GCaMP6-150	de Juan-Sanz et al., 2017	Addgene Plasmid #86918
ER-GCaMP6-210	de Juan-Sanz et al., 2017	Addgene Plasmid #86919
jRCaMP1b	Dana et al., 2016	Addgene Plasmid #63136
GCaMP6f	Chen et al., 2013	Addgene Plasmid #40755
OMM-jRCaMP1b	This paper	Addgene Plasmid #127871
OMM-GCaMP6f	This paper	Addgene Plasmid #127874
$Mito^{4x}$-jRCaMP1b	This paper	Addgene Plasmid #127873
$Mito^{4x}$-GCaMP6f	This paper	Addgene Plasmid #127870
Rat MICU3 shRNA resistant	This paper	N/A
$Mito^{4x}$-pHluorin	This paper	N/A
Recombinant DNA for HEK cell only		
OMM-jRCaMP1b-P2A-$Mito^{4x}$-GCaMP6f	This paper	Addgene Plasmid #127872
Voltage-gated Ca^{2+}-channel CaV 2.1	Hoppa et al., 2012	N/A
β1B subunit	Yan et al., 2013	N/A
α2 δ1 subunit	Yan et al., 2013	N/A
psPAX2	Unpublished; Trono Lab (http://addgene.org/12260)	Addgene Plasmid #12260
pMD2.G	Unpublished; Trono Lab http://addgene.org/12259	Addgene Plasmid #12259
pLKO.1 – TRC cloning vector	Moffat et al., 2006	Addgene pPasmid #10878
pLenti CMV GFP Blast (659-1)	Campeau et al., 2009	Addgene Plasmid #17445
Ace-mNeon	Gong et al., 2015	N/A

(*Continued on next page*)

Continued

REAGENT or RESOURCE	SOURCE	IDENTIFIER
Sequence-Based Reagents		
MICU3 shRNA-A-pLKO1	This paper	N/A
MICU3 shRNA-B-pLKO1	This paper	N/A
MCU shRNA-1-pLKO1	This paper	N/A
MCU shRNA-1	Origene Technologies	CAT# TR704979B
MCU shRNA-2	Millipore Sigma	TRCN0000265169
Software and Algorithms		
ImageJ	National Institute of Health	https://imagej.nih.gov/ij
OriginPro 8	OriginLab	https://www.originlab.com/
GraphPad Prism v6	GraphPad	https://www.graphpad.com
MATLAB R2017a	MATLAB Inc.	http://matlabinc.com/

LEAD CONTACT AND MATERIALS AVAILABILITY

We have deposited the main plasmids generated in this work in addgene.org (see Key Resources Table for reference numbers). Further information and requests for resources and reagents should be directed to and will be fulfilled by the Lead Contact Timothy A. Ryan at taryan@med.cornell.edu.

EXPERIMENTAL MODEL AND SUBJECT DETAILS

Animals

All animal-related experiments were performed with wild-type rats of the Sprague-Dawley strain (Charles River code 400, RRID: RGD_734476.) in accordance with protocols approved by the Weill Cornell Medicine IACUC. 1-to 2-day-old rats of mixed gender were sacrificed for further dissection of the hippocampus

Primary Neuronal Culture

Hippocampal neurons were plated on poly-ornithine-coated coverslips, transfected 6-8 days after plating, and imaged 14-21 days after plating as previously described (Ryan, 1999). Neurons were maintained in culture media composed of MEM (Thermo Fisher Scientific 51200038), 0.6% glucose, 0.1 g/L bovine transferrin (Millipore 616420), 0.25 g/L insulin, 0.3 g/L GlutaMAX, 5% fetal bovine serum (Atlanta Biologicals S11510), 2% B-27 (Thermo Fisher Scientific 17504-044), and 4 μm cytosine β-d-arabinofuranoside. Cultures were incubated at 37°C in a 95% air/5% CO_2 humidified incubator for 14–21 days prior to use.

Culture and transfection of "Spiking" HEK293 cells

"Spiking" HEK cells stably expressing the voltage-gated sodium channel Na_V 1.3 and the inward rectifying potassium channel K_{IR} 2.1 were obtained from Dr. Adam Cohen (Harvard University) (Park et al., 2013). K_{IR} 2.1 expression is controlled by a tetracycline Tet-On system. To induce a consistent expression of K_{IR} 2.1, "spiking" HEK cells were incubated in the presence of 5 μg/mL doxycycline for 3-4 days before imaging at 37°C in a 95% air/5% CO_2 humidified incubator. "Spiking" HEK cells were plated in glass coverslips and transfected at a 20% confluency using established calcium phosphate protocols (Kingston et al., 2001), adding a total amount of 7 μg of DNA per 35mm culture plate. For Ca^{2+} signaling experiments, we co-transfected 3 separate plasmids expressing Ca_V2.1, α2 δ1 and β1B together with the indicator of interest, conserving a ratio of DNA amounts of 1.5 / 1 / 1 / 1 respectively. When spiking HEK cells were additionally co-transfected with MICU3, the amount of this plasmid was 2-fold compared to α2 δ1, β1B or the indicator of interest. Cells were imaged 48 h to 72 h after transfection.

METHOD DETAILS

Plasmid Constructs

The following previously published DNA constructs were used: vGLUT1-pHluorin (Voglmaier et al., 2006), Syn-ATP (Rangaraju et al., 2014), ER-GCaMP6-150 and ER-GCaMP6-210 (de Juan-Sanz et al., 2017), α2 δ1 and β1B (Yan et al., 2013), Ca_V2.1 (Hoppa et al., 2012), Ace-mNeon (Gong et al., 2015), MCU-v5-HIS (Baughman et al., 2011) (Addgene 31731) was cloned into the BamH1 and Xho1 sites of the lentiviral expression vector pLenti-MP2 (Enomoto et al., 2013) (addgene 36097). We designed mito^{4x}-GCaMP6f to express 4 consecutive copies of the signal peptide of COX8 (MSVLTPLLLRGLTGSARRLPVPRAKIHSLGDP) and a short linker (RSGSAKDPT) before the sequence of GCaMP6f (Chen et al., 2013), because frequent mislocalization in the cytosol was observed when neurons expressed GCaMPs targeted by a single copy of the signal peptide (Venkatachalam and Cohen, 2014).

To target the pH-sensitive fluorophore pHluorin to the mitochondrial matrix (Mito^{4x}-pHluorin), we replaced GCaMP6f in mito^{4x}-GCaMP6f for pHluorin using AfeI and AgeI sites. For targeting GCaMP6f and jRCaMP1b to the outer membrane of mitochondria, we designed constructs to express the indicators after the first 33 amino acids of human TOM20 (Kanaji et al., 2000) (MVGRNSAIAAGVCGALFIGYCIYFDRKRRSDPN) and a short linker (TGS). To generate a vector to express both mito^{4x}-GCaMP6f and OMM-jRCaMP, we generated by gene synthesis a construct to express under the CMV promoter OMM-jRCaMP1b followed by a short linker (TG), the P2A sequence (ATNFSLLKQAGDVEENPGP) and a short linker (GSTA) that introduces a BamHI site (GGATCC). We subsequently cloned mito^{4x}-GCaMP6f between BamHI and EcoRI sites. We confirmed that this vector successfully expressed and maintained localization of both indicators in HEK cells. For reasons we do not understand this single plasmid for dual expression of the two mitochondrial indicators frequently results in one of the reporters appearing mislocalized when expressed in neurons. As a result, for neurons we used transfection of individual reporter plasmids where appropriate.

To generate an shRNA resistant variant of rat MICU3, we codon-optimized rat MICU3 sequence and introduced at least 5 silent mutations in the regions complementary to shRNA designed (for shRNA A: shRNA resistant MICU3 region GCAATGAAATGGTCGA CAA contains 5 mismatches; for shRNA B: shRNA resistant MICU3 AGAGCTGCACAGTCGTTAA contains 7 mismatches). This construct was used for rescue experiments (Figure S3) and overexpression of MICU3 in spiking HEK cells (Figure 5).

All constructs generated by gene synthesis (GeneArt Gene Synthesis, Thermo Fisher Scientific) were codon-optimized for rat expression using the GeneOptimizer tool (Thermo Fisher Scientific). We used the pLKO.1 vector (Moffat et al., 2006)(Addgene 10878) for expression of shRNAs against rat MCU which was obtained from Origene Technologies (shRNA-1: TR704979B, GCTACCTTCTCGGCGAGAACGCTGCCAGTT), and Millipore Sigma (shRNA-2: TRCN0000265169, CATGGCCATGTATGCG TATTT), as well as rat MICU3 (shRNA A: GAAACGAGATGGTGGATAA; shRNA B: GGAACTTCATAGCAGATAA).

Lentiviral Production and Application

HEK293FT cells were transfected by calcium phosphate with lentiviral constructs along with the associated packaging plasmids psPAX2 (a gift of Didier Trono, Addgene 12260) and pMD2.G (a gift of Didier Trono, Addgene 12259). 16 h post transfection, media was changed to serum free viral production media: Ultraculture (Lonza), 1% (v/v) Penicillin-Streptomycin/L-glutamine, 1% (v/v) 100 mM sodium pyruvate, 1% (v/v) 7.5% sodium bicarbonate and 5 mM sodium butyrate. HEK293FT supernatants were collected at 46 h post transfection and filtered through a 0.45 μm cellulose acetate filter. Viral supernatants were then concentrated and buffer exchanged into neuronal culture media (MEM, 5% FBS, 4 μM ARA-C, 2% B-27) using an Amicon Ultra-15 100K MW Cutoff Centrifugal Filter (Millipore). Samples were aliquoted and stored at −80°C until use.

Viral aliquots were functionally titrated using parallel preparation of GFP-expressing viral particles (Campeau et al., 2009)and determining the volume of lentivirus required to achieve ~100% transduction of hippocampal or cortical cultures. When genomic titer determination (Lenti-X qRT-PCR Titration Kit, Takara) was performed on some viral preparations with qPCR, the functional titer was found to be equivalent to ~10^6 GC (genome copies)/mL.

For imaging experiments, lentivirus was added to neurons 3-4 days *in vitro* and after 3 days of infection, media exchange was performed. Due to the long half-life of MCU (Cohen et al., 2013; Heo et al., 2018) all experiments were performed at least 10 days after viral transduction to ensure protein knockdown.

Live Imaging of Neurons

Imaging experiments were performed on a custom-built laser illuminated epifluorescence microscope with an Andor iXon+ camera (model #DU-897E-BV). TTL-controlled Coherent OBIS 488 nm and 561 nm lasers were used for illumination. Images were acquired through a 40X 1.3 NA Fluar Zeiss objective. Coverslips were mounted in a laminar flow perfusion chamber and perfused with Tyrodes buffer containing (in mM) 119 NaCl, 2.5 KCl, 2 $CaCl_2$, 2 $MgCl_2$, 50 HEPES (pH 7.4), 5 glucose or 1.25 lactate and 1.25 pyruvate, supplemented with 10 μM 6-cyano-7nitroquinoxalibe-2, 3-dione (CNQX), and 50 μM D,L-2-amino-5phosphonovaleric acid (APV) (both from Sigma-Aldrich) to inhibit post-synaptic responses. Action potentials were evoked in neurons with 1 ms pulses creating field potentials of ~10 V/cm via platinum–iridium electrodes. Temperature was maintained at 37°C using a custom-built objective heater jacket in all experiments except for those shown on Figure 3, which were performed at 26°C to eliminate the previously-observed modulation of presynaptic Ca^{2+} entry triggered by CPA at 37°C (de Juan-Sanz et al., 2017; Emptage et al., 2001; Liang et al., 2002).

Luminescence imaging of the presynaptic ATP reporter, Syn-ATP, was performed as previously described (Rangaraju et al., 2014). Although all our ATP measurements are pH-corrected as previously described (Rangaraju et al., 2014), given that we did not observe significant differences in pH changes (data not shown) when comparing wild type neurons and MCU/MICU3 KD neurons, here we do not propagate errors of pH measurements into the final error shown in ATP measurements.

NH_4Cl solution for alkalization of pHluorin-containing vesicles had a similar composition as Tyrodes buffer except it contained (in mM): 50 NH_4Cl and 69 NaCl. Ionomycin (Alomone Labs) at 500 μM final concentration was applied in pH 6.9 Tyrodes buffer containing 4mM $CaCl_2$. For experiments performed in the absence of glucose, a glucose-free NH_4Cl solution was used. Neurons were incubated for 5 min with 2 μM oligomycin A (Enzo Life Sciences) in Tyrodes buffer to block mitochondrial ATP production.

Live Imaging of "Spiking" HEK293 cells

Imaging experiments were performed in the same custom-built setup used for neurons. "Spiking" HEK cells were imaged at a confluency of ~75%, which helps to reduce their previously reported spontaneous firing behavior induced at confluency by intercellular

electrical coupling through gap junctions (Park et al., 2013). Single action potentials were evoked on-demand in "Spiking" HEK cells with a 10 ms pulse, creating a field potential of ~10 V/cm via platinum–iridium electrodes. Cells were imaged in the same Tyrodes buffer as neurons, except we removed CNQX and APV and varied Ca^{2+} concentrations as indicated, ranging from 0.5 mM to 4 mM with the corresponding change in $MgCl_2$ concentrations to maintain osmolality in each buffer. Transfected areas of the dish were randomly chosen and typically contain 5 to 15 transfected cells. To image voltage changes in the HEK plasma membrane using Ace-mNeon (Figure S2) (Gong et al., 2015), images were collected at 100 Hz. For Ca^{2+} signaling experiments cells were imaged at 1 Hz. We confirmed that in "spiking" HEK cells, Ca^{2+} responses induced by field stimulation are stable for at least 30 min (not shown). When imaging two different Ca^{2+} indicators in the same HEK cell (Figure 4), we first imaged jRCaMP1b-based indicators, waited 2 min and imaged GCaMP-based indicators in the same experimental conditions. The power of the 488 nm laser at the back aperture was never more than 0.3 mW, as we have found that jRCaMP1b becomes unresponsive after strong 488 illumination. Whereas mito^{4x}-GCaMP6f appeared well localized in HEK mitochondria, we observed OMM-jRCaMP1b mislocalization in certain cases. HEK cells where the OMM-jRCaMP1b pattern did not match the mito^{4x}-GCaMP6f were excluded from the analysis.

RNA Isolation and Quantitative PCR

Total RNA was isolated from primary dissociated cortical neuron cultures using TRIzol (Thermo Fisher Scientific) and chloroform (Sigma-Aldrich) along with RNeasy Mini Kits (QIAGEN). RNA was reverse transcribed using SuperScript IV VILO Master Mix with ezDNase Enzyme using manufacturer recommended protocol. cDNA was used in qPCR reactions containing TaqMan Fast Advanced Master Mix (Thermo Fisher Scientific) and TaqMan Gene Expression Assays (Thermo Fisher Scientific). Relative mRNA expression was determined by normalizing to *Actb* using the $\Delta\Delta C_t$ method. Specific TaqMan assay information can be found in the Key Resources Table.

Experimental design

No statistical methods were used to predetermine sample size. The experiments were not randomized. The investigators were not blinded to allocation during experiments and outcome assessment. An inclusion and exclusion criteria was used in the analysis of "Spiking" HEK293 Cells to: 1) avoid overestimation of $\Delta F/F_0$ when baseline fluorescence of the sample (F_0) is close to background fluorescence, 2) use only cells that were not spontaneously spiking and 3) include only reliable outer membrane responses. Details can be found in the Quantification and Statistical Analysis section. An inclusion and exclusion criteria was used in the analysis of mitochondrial and ER Ca^{2+} measurements to avoid overestimation of $\Delta F/F_0$ when baseline fluorescence of the sample (F_0) is close to background fluorescence. We set an arbitrary threshold applied to all mito4x-GCaMP6f and ER-GCaMP6-150 experiments in neurons such that F_0/background > 1.25 to be included for further analysis. Experiments were replicated with neurons from at least 3 independent primary culture preparations or HEK293 cells from 3 independent passages.

QUANTIFICATION AND STATISTICAL ANALYSIS

Image Analysis and Statistics

Images were analyzed using the ImageJ plugin Time Series Analyzer where ~10-20 regions of interest (ROIs) of ~2 μm corresponding to responding synaptic boutons were selected and the fluorescence was measured over time. All fitting was done with OriginPro v8 as previously described (Balaji and Ryan, 2007). Statistical analysis was performed with OriginPro v8 and GraphPad Prism v6.0 for Windows. In most experiments, as indicated in the figure legends, the nonparametric Mann–Whitney U test was used to determine the significance of the difference between two unpaired conditions, as we did not assume that the distributions of our two unpaired datasets follow a normal distribution. For paired comparison of responses, the nonparametric Kolmogorov-Smirnov test was used, as we did not assume that the distributions of our two paired datasets follow a normal distribution. $p < 0.05$ was considered significant and denoted with a single asterisk, whereas $p < 0.01$, $p < 0.001$ and $p < 0.0001$ are denoted with two, three, and four asterisks, respectively. The n value, indicated in the figure legends for each experiment, represents the number of cells imaged.

Quantification of Synaptic Vesicle Fractional Retrieval Block

Endocytic time constants were calculated as previously described by fitting the fluorescent change after the stimulus to a single exponential decay (Armbruster and Ryan, 2011). The fractional retrieval block in endocytosis of vGLUT1-pH was calculated as the fraction of ΔF remaining after 2 times the average endocytic time constant of the control (2tau) to maximum ΔF at the end of stimulation ($\Delta F_{2tau}/\Delta F_{max}$).

In the case of oligomycin A treatment (Figures 1C–1E), individual (not average) endocytic time constants before treatment was used for each cell.

Analysis of "Spiking" HEK293 Cells

Dynamic responses were analyzed using the ImageJ plugin Time Series Analyzer, placing manually-drawn single regions of interest (ROIs) per cell. Fluorescence signals in response to electrical activity (ΔF) were normalized to the resting fluorescence (F_0) indicated as ΔF/F throughout. The F_0 value was additionally corrected for background autofluorescence measured in a nearby non-transfected region. For Ace-mNeon experiments, we averaged 10-15 single-stimulation trials to reduce signal-to-noise in our measurements. For

Ca^{2+} signaling experiments, data were obtained from single trials and we applied inclusion and exclusion criteria with the following elements: 1) To avoid overestimating ΔF/F which would arise in cells with low F_0 values, we set an arbitrary threshold such that F_0/background > 1.25 to be included for further analysis. 2) As spiking HEK cells may present spontaneous responses (Park et al., 2013), we include cells that are silent before stimulation by selecting cells whose standard deviation of their baseline fluorescence is low, excluding any cells with a standard deviation of the ΔF/F before stimulation higher than 0.075. 3) Lastly, we only include cells with a response of OMM-jRCaMP1b 3 times higher than the standard deviation of the baseline fluorescence, allowing us to only use cell with reliable outer membrane responses. Criteria #3 is not applied to mito^{4x}-GCaMP6f responses as arbitrarily small responses must be included to determine the responsive of the matrix signal for a given OMM signal.

Mitochondrial Ca^{2+} measurements using mito^{4x}-GCaMP6f

For mitochondrial Ca^{2+} signaling experiments, data were obtained from imaging at 5 Hz (Figures 2, 4, and 5) from a single trial or an average of 3 trials (Figure 3). We found that in some cases as previously reported with similarly targeted reporters (Greotti et al., 2019), a small fraction of mito^{4x}-GCaMP6f appeared mislocalized in the cytosol, which would contaminate the quantification of peak mitochondrial responses. We leveraged the kinetic differences of cytosolic and mitochondrial Ca^{2+} responses to quantify exclusively mitochondrial Ca^{2+}. Since mitochondrial responses persist much longer than those in the cytosol, we chose a 1 s delay after the stimulus, when cytosolic Ca^{2+} has returned to baseline, as a measure of the matrix response to ensure that it is not corrupted by any contribution from mislocalized probes. For clarity, in figures, we show responses that did not present mislocalization.

Resting mitochondrial Ca^{2+} estimates using mito^{4x}-GCaMP6f

This method relies on the experimental measurement Mito^{4x}-GCaMP6f fluorescence at saturating [Ca^{2+}] in mitochondria (F_{max}), which is obtained by applying Tyrode's solution containing 500 μM ionomycin, 4 mM $CaCl_2$ and 0 mM $MgCl_2$ at pH 6.9 buffered with 25 mM HEPES. Knowing the *in vitro* characteristics of GCaMP6f (Chen et al., 2013), baseline mitochondrial [Ca^{2+}] (Ca_r) is calculated from F_{max} using the following equation:

$$[Ca]_r = K_d \left(\frac{F_r/F_{max} - 1/R_f}{1 - F_r/F_{max}} \right)^{1/n} \quad \text{(Eq 1)}$$

K_d is the affinity constant of the indicator, F_r is the measured fluorescence at rest, R_f is the dynamic range (F_{sat}/F_{apo}) and *n* is the Hill coefficient. Ionomycin application does not produce a change in mitochondrial matrix pH (data not shown; initial pH 7.203; ionomycin-treated mitochondria pH 7.206). Neurons with apparent cytosolic mislocalization of mito^{4x}-GCaMP6f were excluded from these estimates.

Mitochondrial pH measurements

Mitochondrial pH measurements were made using mito^{4x}-pHluorin and axonal mitochondria were imaged. Neurons were briefly perfused with a Tyrode's solution containing 100 mM NH_4Cl buffered at pH 7.4 25 mM HEPES, which equilibrated mitochondrial pH to 7.4. The fluorescence value when pH stabilizes at 7.4 allows estimating resting mitochondrial pH value using the modified Henderson-Hasselbalch equation:

$$pH = pK_a - log\left[\left(\frac{1 + 10^{pK_a - pH(NH_4Cl)}}{\frac{F_0}{F_{NH_4Cl}}} \right) - 1 \right] \quad \text{(Eq 2)}$$

pKa is the pKa of pHluorin, 7.1, pH (NH_4Cl) is the pH of 100 mM NH_4Cl buffer used, F_0 is the fluorescence of mito^{4x}-pHluorin measured before NH_4Cl perfusion, F_{NH4Cl} is the fluorescence of mito^{4x}-pHluorin measured upon NH_4Cl perfusion when signal is stable.

DATA AND CODE AVAILABILITY

This study did not generate new code. The data that support the findings of this study are available from the Lead Contact upon reasonable request.